

OPTICAL IMAGE PROCESSING

PACS numbers: 42.87.–d; 42.65.–k
DOI: 10.1070/QE2012v042n04ABEH014712

Analysis of the process of visualisation of transparent objects using the phase-contrast method with a photothermal Zernike cell

E.L. Bubis, A.Z. Matveev

Abstract. **Basic characteristics of the process of visualisation of transparent objects using the phase-contrast method with a photothermal Zernike cell are analysed and evaluated. It is shown that, in spite of nonlocality of the process, visualisation is accomplished with the resolution close to the diffraction limit. The results of the visualisation process analysis in the scheme with a photothermal sell are compared with those obtained in a similar scheme with a Zernike cell based on the local Kerr nonlinearity.**

Keywords: *nonlinear optics, thermal self-action, phase contrast.*

1. Introduction

The phase-contrast method, proposed by F. Zernike in 1934, is used to detect weak phase perturbations in a light wave passed through an investigated object or medium. This method provides linear transformation of phase modulation into the amplitude one. The Zernike method is used to visualise transparent objects and structures, as well as to analyse the wave front of optical beams with weak phase inhomogeneities [1–3]. The visualisation is implemented by placing a Zernike plate (filter) in the focal plane of the objective. The role of the Zernike filter is to introduce a selective phase shift $\Theta_Z \approx \pm\pi/2$ between the direct light (also called 'nondiffracted light', 'zero diffraction order', and 'zero spatial frequency') and diffracted light (the terms 'diffraction spectrum' and 'higher spatial harmonics' are also used) [2, 4, 5]. In the nonlinear phase-contrast method this phase shift is implemented in a nonlinear medium (nonlinear filter, or Zernike cell) [3, 6–14]. As compared with the schemes using conventional linear Zernike cells, the nonlinear phase-contrast schemes require much less alignment, are easily tuneable, and the required phase shift is achieved by choosing an appropriate intensity of light, entering the nonlinear medium.

The Zernike filters based on the thermal nonlinearity mechanism were implemented in work [8–10, 14–16]. However, in the authors' opinion, up to date the properties of such cells are not analysed in detail. Among nonlinear phase-contrast schemes the schemes with photothermal Zernike cells possess certain advantages. The required level of radiation power in these cells corresponds to the initial stage of beam thermal self-action development in the medium. The present mechanism possesses the lowest threshold for cw and quasi-cw laser radiation in simple, easily available media.

In the present paper we report a numerical analysis of the basic properties of the phase-contrast scheme for visualising transparent objects using a photothermal Zernike filter based on an absorbing medium with a thermal nonlinearity mechanism. The nonlocality of the medium response is taken into account. Within the paraxial approximation the transfer characteristic function and the spatial resolution of the considered scheme are determined. Comparative analysis of properties of a photothermal Zernike cell and a Zernike cell based on inertialess nonlinearity is presented.

2. Setting of the problem

We analysed the phase-contrast scheme for visualising transparent (phase) objects, presented in Fig. 1. The $2f$-to-$2f$ image transfer was considered, f being the focal length of the objective lens. The initial field $A_{in}(x, y)$ was specified in the plane where the transparent object was located. The output field $A_{out}(x, y)$ was sought for in the image plane. To calculate the output field $A_{out}(x, y)$, the diffraction Fresnel–Kirchhoff integral in the paraxial approximation was used. It was assumed that the studied transparent object is illuminated with a laser beam having a Gaussian intensity profile and plane wave front. In the focal plane of the objective lens (*1*) the photothermal Zernike filter (*2*) was placed. A part of the radiation was absorbed in the cell, implemented as a cylindrical solid sample, from which the heat was removed in the radial direction, thus giving rise to inhomogeneous heating of the cell (*2*).

In the analysis it was also assumed that the size and intensity of the beam are constant within the cell, i.e., the absorption losses are small and the cell is optically thin. Moreover, in the calculation of the temperature profile $T(r)$ the light intensity distribution within the Zernike cell was assumed to

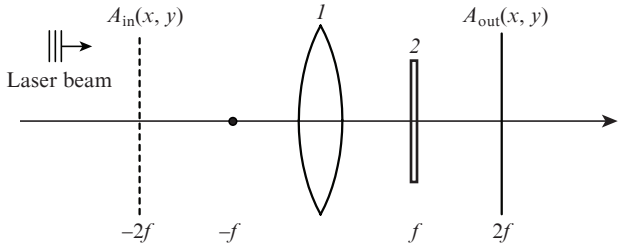

Figure 1. Analysed phase-contrast scheme for visualising transparent objects: (*1*) objective; (*2*) photothermal Zernike filter.

E.L. Bubis, A.Z. Matveev Institute of Applied Physics, Russian Academy of Sciences, ul. Ul'yanova 46, 603950 Nizhnii Novgorod, Russia; e-mail: bel@appl.sci-nnov.ru, amatveev@appl.sci-nnov.ru

Received 1 September 2011; revision received 14 December 2011
Kvantovaya Elektronika **42** (4) 361–366 (2012)
Translated by V.L. Derbov

be Gaussian. In other words, it was assumed that the presence of the transparent object does not practically change the distribution $T(r)$. The radial stationary distribution of temperature in the cell was found from the solution of the heat conduction equation, which in the cylindrical coordinate system takes the form

$$\frac{1}{r}\frac{\mathrm{d}}{\mathrm{d}r}\left(r\frac{\mathrm{d}T}{\mathrm{d}r}\right) = -\frac{2\alpha P_{\mathrm{in}}}{\pi K w_{\mathrm{f}}^2}\exp\left(-\frac{2r^2}{w_{\mathrm{f}}^2}\right). \quad (1)$$

Here α is the coefficient of linear absorption; P_{in} is the power of radiation, incident on the cell; K is the heat conduction coefficient; w_{f} is the radius of the Gaussian beam (at the e^{-2} level of the maximal intensity) in the focal plane of the lens.

Under the boundary conditions $T(r = r_0) = 0$, where r_0 is the radius of the Zernike cell, the considered heat conduction equation (1) has the rigorous solution [17]:

$$\Delta T(r) = T(r) - T(0) = -\frac{\alpha P_{\mathrm{in}}}{4\pi K}\mathrm{Ein}(X),$$
$$T(0) = \frac{\alpha P_{\mathrm{in}}}{4\pi K}\mathrm{Ein}(X_0), \quad (2)$$

in which

$$X = \frac{2r^2}{w_{\mathrm{f}}^2}; \quad X_0 = \frac{2r_0^2}{w_{\mathrm{f}}^2}; \quad \mathrm{Ein}(X) = [\mathrm{E}_1(X) + \ln(X) + \gamma];$$

$\mathrm{E}_1(X)$ is the exponential integral function; $\gamma = 0.577\ldots$ is the Euler constant [18].

Due to nonuniform heating, a nonuniform profile of the refractive index n is induced in the cell, giving rise to phase mismatch of spatial harmonics and visualisation of the object image. The nonuniform phase $\Delta\varphi(r)$, introduced into the beam by the Zernike cell, is determined by the distribution (2) of the temperature $\Delta T(r)$, as well as by a number of parameters that characterise the medium of the Zernike cell and the heating beam:

$$\Delta\varphi(r) = \varphi(r) - \varphi(0) = k_0\beta L\Delta T(r) = B_{\mathrm{T}}\mathrm{Ein}\left(\frac{2r^2}{w_{\mathrm{f}}^2}\right), \quad (3)$$

where L is the length of the Zernike cell; $\beta = \mathrm{d}n/\mathrm{d}T + (1/L) \times (\mathrm{d}L/\mathrm{d}T)(n-1)$; $k_0 = 2\pi/\lambda_0$; λ_0 is the wavelength of the incident beam;

$$B_{\mathrm{T}} = \frac{1}{2}\frac{P_{\mathrm{in}}}{P_{\mathrm{th}}}; \quad P_{\mathrm{th}} = \frac{2\pi K}{k_0\beta L\alpha}; \quad (4)$$

P_{th} is the threshold power of thermal self-(de)focusing of the beam in a short-path medium. The visualisation process is determined by the phase difference $\Delta\varphi(r)$ introduced into the angular spectrum of the phase object. According to Eqn (3), the value of $\Delta\varphi(r)$ depends on the parameters B_{T} and w_{f} and does not depend on the size r_0 of the Zernike cell. The latter statement is valid, if the angular spectrum of the phase object does not spread beyond the limits of the cell, which is implied in the following considerations.

Provided that the temperature distribution $\Delta T(r)$ is known and, correspondingly, the phase difference $\Delta\varphi(r)$, introduced into the beam by the Zernike cell, is known as well, one can use the diffraction integral to evaluate numerically the intensity distribution for simple phase objects in the plane of their image. The diffraction integral was evaluated using the fast Fourier transform with the resolution 1024×1024 elements. The lens (*1*) was assumed to have an infinite aperture in all cases except the analysis of the Zernike filter resolution power.

In the experiments [9–11, 14] a liquid-based Zernike cell was used. The model described above may be applied to the analysis of operation of the scheme with a liquid-based Zernike cell provided that the convection is absent. Note that for the majority of optical glasses $\mathrm{d}n/\mathrm{d}T > 0$, while in liquids and gases $\mathrm{d}n/\mathrm{d}T < 0$ (see, e.g., [19]). In the scheme with the corresponding Zernike cell this means a change in the image contrast sign.

3. Discussion of results

Let us assume that the transparent low-contrast object introduces a small phase increment $\varphi(x, y)$ into the illuminating radiation. In this case the linear phase-contrast Zernike method yields the following expression for the light intensity distribution in the image plane [2]

$$I_{\mathrm{out}}(x, y) \propto [1 + 2\varphi(x, y)\sin\Theta_{\mathrm{Z}}]. \quad (5)$$

From this expression it follows that the visualisation takes place at any nonzero value of the phase shift Θ_{Z} between the zero-order (direct light) and higher-order spatial harmonics (diffracted light), and the maximum of sensitivity is attained at $\Theta_Z = \pm\pi/2$. In this case the transfer characteristic function of the given Zernike cell, i.e., the dependence $I(\varphi)$, is linear and has the slope ratio equal to 2. The linear transfer characteristic function guarantees correct visualisation of the phase object.

Let us discuss the possible problems arising with nonlinear Zernike cells. If the required phase shift occurs in a nonlinear medium, then even in a local Kerr medium, for which $\Delta n = n_2 I$, the attainment of the required phase shift $\pi/2$ is accompanied by self-action effects. One can expect that they will impair the image quality. In the case of a photothermal Zernike cell additional problems may arise due to nonlocality of the heating process, because of which the temperature distribution $\Delta T(r)$ in the Zernike cell and, hence, the distribution of the phase shift $\Delta\varphi(r)$ introduced into the beam, do not repeat the distribution of the heating light beam. Figure 2 shows typical distributions of the temperature [curve (*1*)] and the intensity of heating light beam [curve (*2*)] inside the Zernike cell. There are two features of the distribution $T(r)$ able to impair the quality of the phase object visualisation. First, the distribution of temperature $T(r)$ is broader than the distribution of the heating light beam intensity $I(r)$. Second, this distribution demonstrates far-spreading slowly-descending wings. All this means that the photothermal Zernike cell not only introduces a phase shift into the zero spatial har-

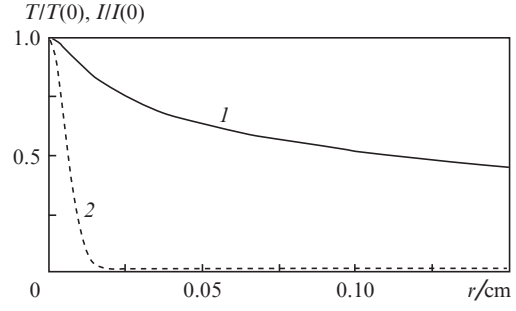

Figure 2. Normalised distributions of the temperature T (*1*) and intensity I (*2*) inside the photothermal Zernike filter.

monic, but also changes the phase relations in the angular spectrum of the phase object, due to which the quality of visualisation becomes worse.

Below we present the results of numerical calculations. We assumed the focal length of the lens (*1*) (Fig. 1) to be f = 100 cm, the wavelength of the Gaussian beam illuminating the object λ = 0.63 μm, its radius w_0 = 0.18 cm (sampling increment 27 μm), unless particularly specified, the radius of the photothermal Zernike cell, placed in the focal plane of the lens, r_0 = 2.0 cm. Note that the radius of the illuminating Gaussian beam in the focal plane of the lens is w_f = 111 μm.

Consider a transparent object in the form of a phase slit, described by the function

$$\varphi_{sl}(x) = \frac{\varphi_0}{2}\left[\mathrm{erf}\left(\frac{x + 0.5d_{sl}}{w_{erf}}\right) - \mathrm{erf}\left(\frac{x - 0.5d_{sl}}{w_{erf}}\right)\right], \qquad (6)$$

where erf(x) is the probability integral; d_{sl} is the slit width; w_{erf} is the distance within which the phase jump by φ_0 occurs. As an example of visualising the phase slit using a thermal Zernike cell, Fig. 3a presents the intensity distribution I_{out}, obtained in the image plane. *A priori* it is known that the illuminating beam is Gaussian. This information allows reconstruction of the phase distribution in the initial phase object: $I_{norm}(x) = I_{out}(x)/f_g(x)$, $\Phi(x) = I_{norm}(x) - 1$ [see Eqn (5)], where $f_g(x) = f_{gin}(x) = \exp(-2x^2/w_0^2)$, $\Phi(x)$ is the quantity, proportional to the reconstructed phase distribution (phase image). If a more precise analysis is desirable, then it is preferable to scale I_{out} to the intensity distribution of the illuminating light beam in the image plane in the absence of the phase object $f_{gout}(x)$. In most cases the authors used this kind of scaling. Below by the term 'reconstruction' we mean just the simplest mathematical procedure, described here.

Figure 3b presents the reconstructed distributions of phase $\Phi(x)$ in the cross-section plane y = 0 for a number of slits having different widths. The obtained image satisfactorily reproduces the initial phase slit, although some distortions, typical for the edge enhancement effect, are present in the image. The data, presented in Fig 3b, confirm the low-frequency nature of the observed distortions. Their origin is associated with the nonlocality of the thermal Zernike cell response, due to which the distribution $T(r)$ does not repeat the narrow distribution of the heating beam amplitude in the focal plane of the lens, where the Zernike cell is located. In the distribution $T(r)$ (see Fig. 2) two regions can be specified, namely, the central core and the slowly descending wings. If the central core of the distribution $T(r)$ is comparable with the size of the angular spectrum of the phase object in the focal plane of the lens, then low-frequency distortions will be present in the reconstructed phase distribution. They are due to the phase difference between the low-frequency and high-frequency components of the angular spectrum of the phase object, introduced by the thermal Zernike cell. These distortions in the reconstructed image of the phase object formally manifest themselves as the edge enhancement effect. In this effect, aimed at enhancing boundaries between light and dark parts of the image, a small region, adjacent to the boundary is made darker from the dark side and lighter from the light one. In most cases this effect is implemented by adding either the first, or the second derivative to the initial intensity distribution. In other words, high-frequency distortions are added. In the case of thermal Zernike cell the edge enhancement results from distortions in low frequency reproduction.

By the example of the phase slit let us analyse a number of Zernike cell characteristics. In the curve $\Phi(x)$, presented in Fig. 3b, one can select three characteristic points, denoted by Φ_{max}, Φ_{min}, and Φ_0. Let us associate the phase jump φ_0 at the original slit with the quantity $\Phi_0 = \Phi_{min} - \Phi_{max}$, if $\varphi_0 < 0$, and with the quantity $\Phi_0 = \Phi_{max} - \Phi_{min}$, if $\varphi_0 > 0$. The process of the object visualisation will be characterised using the coefficient $\varepsilon = \Phi_0/\varphi_0$, describing the transfer of the original phase into the phase image. As mentioned above, correct reproduction of the phase object requires using the linear region of the transfer characteristic of Zernike cell, where ε is independent of φ_0. A characteristic dependence $\varepsilon(\varphi_0)$ is presented in Fig. 4a. Within the limits $|\varphi_0| \leqslant 1$ rad one can consider ε to be independent of φ_0. Further studies of the thermal Zernike cell were performed within the linear part of the transfer characteristic.

In correspondence with Eqn (5) the transfer constant ε is determined by the phase difference Θ_Z between the direct and the diffracted light, introduced by the thermal Zernike cell. The analysis of Eqn (3), describing the phase difference $\Delta\varphi$, introduced by the thermal Zernike cell, shows that in the case of slit visualisation the quantity ε depends on three parame-

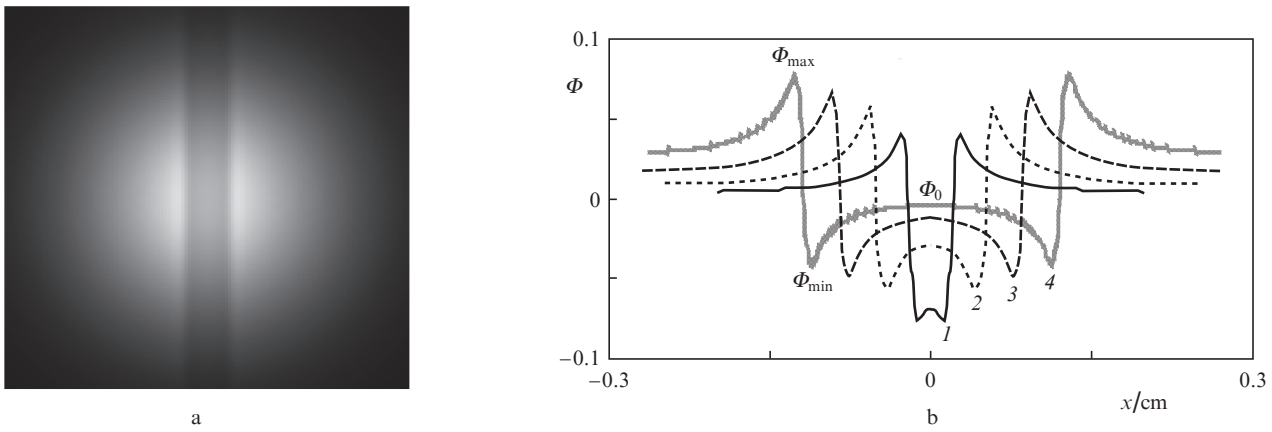

Figure 3. Visualisation of the phase slit using a photothermal Zernike filter. Distribution of the intensity in the image plane I_{out}, obtained upon visualisation of the phase slit having the width d_{sl} = 0.44 cm with the phase jump $\varphi_0 = -0.1$ rad; the parameter B_T = 0.15 (a). Reconstructed distributions of phase $\Phi(x)$ in the cross-section plane y = 0 for slits having the width 0.04 (*1*), 0.1 (*2*), 0.17 (*3*), 0.24 cm (*4*) and the phase jump $\varphi_0 = -0.1$ rad; the parameter B_T = 0.15 (b).

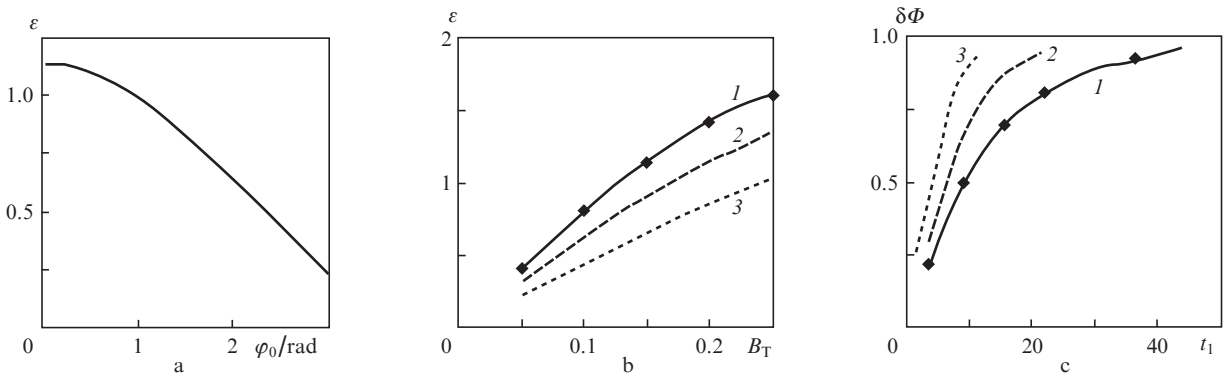

Figure 4. Characteristics of the photothermal Zernike filter. Dependence of the transfer constant ε on the phase jump φ_0 at the original phase slit having the width $d_{sl} = 0.1$ cm for $B_T = 0.15$, $w_{erf} = 55$ μm (a). Dependence of the transfer constant $\varepsilon(B_T)$ (b) and the relative error of the visualisation process $\delta\Phi(t_1)$ (c), obtained at $t_0 = 32.9$ [(*1*); $w_0 = 0.18$ cm, $w_{erf} = 55$ μm], $t_0 = 16.5$ [(*2*); $w_0 = 0.18$ cm, $w_{erf} = 109$ μm] $t_0 = 8.2$ [(*3*); $w_0 = 0.18$ cm, $w_{erf} = 219$ μm]. Diamonds label the values of ε, obtained at $t_0 = 32.9$, $w_0 = 0.36$ cm, and $w_{erf} = 109$ μm.

ters, B_T, $t_0 = w_0/w_{erf}$, and $t_1 = d_{sl}/w_{erf}$. The results of numerical calculations indicate a very weak dependence of ε on the parameter t_1 within the studied interval of t_1 values from 7 to 44. In the first approximation one can consider ε to be independent of t_1 within this interval. The dependences on two remaining parameters are presented in Fig. 4b Curve (*1*) is obtained at $w_0 = 0.18$ cm, $w_{erf} = 55$ μm ($t_0 = 32.9$). The diamonds label the values of ε, obtained with the same $t_0 = 32.9$, but for different values of w_0 and w_{erf}. It is seen that these data perfectly fit with the curve (*1*), which confirms the functional dependence of ε not upon the variables w_0 and w_{erf} separately, but upon their ratio $t_0 = w_0/w_{erf}$. It follows from Fig. 4b that using the thermal Zernike cell one can approach the transfer constant values close to the theoretical limit $\varepsilon = 2$.

Besides the transfer constant ε, the error arising in the visualisation process is also an important characteristic of this process. The process of slit visualising will be characterised by the absolute $\Delta\Phi$ and relative $\delta\Phi$ errors: $\Delta\Phi = \Phi_{max} + (\Phi_0 - \Phi_{min}) = (\Phi_{max} - \Phi_{min}) + \Phi_0$, $\delta\Phi = \Delta\Phi/(\Phi_{max} - \Phi_{min})$, if $\varphi_0 < 0$ (see Fig. 3b), or $\Delta\Phi = \Phi_0 - (\Phi_{max} - \Phi_{min})$, $\delta\Phi = \Delta\Phi/(\Phi_{max} - \Phi_{min})$, if $\varphi_0 > 0$. Similar to ε, these errors (both relative and absolute) depend on three parameters B_T, $t_0 = w_0/w_{erf}$, and $t_1 = d_{sl}/w_{erf}$. Numerical calculations show that under the variation of B_T from 0.05 to 0.25 the relative error $\delta\Phi$ is practically independent of the parameter B_T. The dependences of $\delta\Phi$ on the parameters t_0 and t_1 are shown in Fig. 4c. Curve (*1*) is obtained at $w_0 = 0.18$ cm, $w_{erf} = 55$ μm ($t_0 = 32.9$). Diamonds label the values of $\delta\Phi$, obtained at the same $t_0 = 32.9$, but with $w_0 = 0.36$ cm and $w_{erf} = 109$ μm. It is seen that these points lie on curve (*1*), which confirms the functional dependence of $\delta\Phi$ on the ratio $t_0 = w_0/w_{erf}$. From the presented dependence $\delta\Phi(t_1)$ the conclusion follows that the narrower the slit, the smaller the relative error and the better the reconstruction of the initial object phase. This qualitative conclusion also agrees with the data, presented in Fig. 3b. Moreover, from the data of Fig. 4c it follows that for the visualisation of phase objects using thermal Zernike cells the relative level of low-frequency distortions amounts to tens per cent.

The results of processing of the experimentally visualised images of some simple phase objects demonstrated the presence of the edge enhancement effect in all cases [14], which is an evidence of correctness of the presented model and numerical calculations.

As mentioned above, a specific feature of the thermal Zernike cell is the nonlocality of its response to the action of light. Probably, the best version of a nonlinear Zernike cell could be the one using a nonlinear medium with instantaneous local response. The example of such medium is, e.g., a medium with cubic nonlinearity. In such a medium the dependence of the refractive index n on the intensity of light I has the form

$$n(\boldsymbol{r}, t) = n_0 + n_2 I(\boldsymbol{r}, t). \tag{7}$$

Let us compare the characteristics of Zernike cells with cubic and thermal nonlinearity. Consider a Zernike cell with cubic nonlinearity. We shall characterise it with the parameter $\Theta_Z = k_0 n_2 I_0 L = B$ [compare with Eqn (4)], where I_0 is the intensity of the illuminating Gaussian beam in its centre, B is the break-up integral. The distribution of intensity I_{out} in the image plane, obtained in the case of phase slit visualisation, is presented in Fig. 5a [curve (*1*), $\Theta_Z = B = \pi/2$]. For comparison, the same figure shows the distribution of intensity f_{gin} of the illuminating Gaussian beam in the absence of the slit and Zernike cell [curve (*2*)]. Note that the presence of the Zernike cell leads to a decrease in the intensity in the centre of the distribution and its growth at the edges. Here we meet a manifestation of self-action. When using a thermal Zernike cell the visualisation with the transfer constant $\varepsilon \sim 1$ is implemented at the parameter $B_T \sim 0.1$, when the self-action of the illuminating beam is inessential. Figure 5b presents the normalised distribution of intensity $I_{norm}(x) = I_{out}(x)/f_{gin}(x)$, where $f_{gin}(x) = \exp(-2x^2/w_0^2)$. The visualisation of the transparent object using the Zernike cell with cubic nonlinearity is better than that using the thermal cell (see Fig. 3b). The curve $I_{norm}(x)$ in Fig. 5b is characterised by two intensity values, the maximal I_{max} and the minimal I_{min}. The difference of I_{max} from unity is due to the self-action of radiation in the Zernike cell. The greater the B, the stronger the self-action and the smaller I_{max}. Such a behaviour is reflected by the dependence $I_{max}(B)$, presented in Fig. 5c [curve (*1*)]. The quantity $\Phi_0 = (I_{min} - I_{max})$ characterises the phase jump φ_0 in the initial object, it depends both on the parameter B of the cell and on the phase jump φ_0 at the initial slit. The dependence $\Phi_0(\varphi_0)$ at $|\varphi_0| < 1$ is close to linear with the slope ratio ε depending on B. The determined dependence $\varepsilon(B)$ is presented in Fig. 5c [curve (*2*)]. From this dependence it follows that the maximal response $\varepsilon \approx 1$ is attained at $B = 0.8\pi$.

Resolving power is one more important characteristic of an object visualisation system. Let us study the resolution in

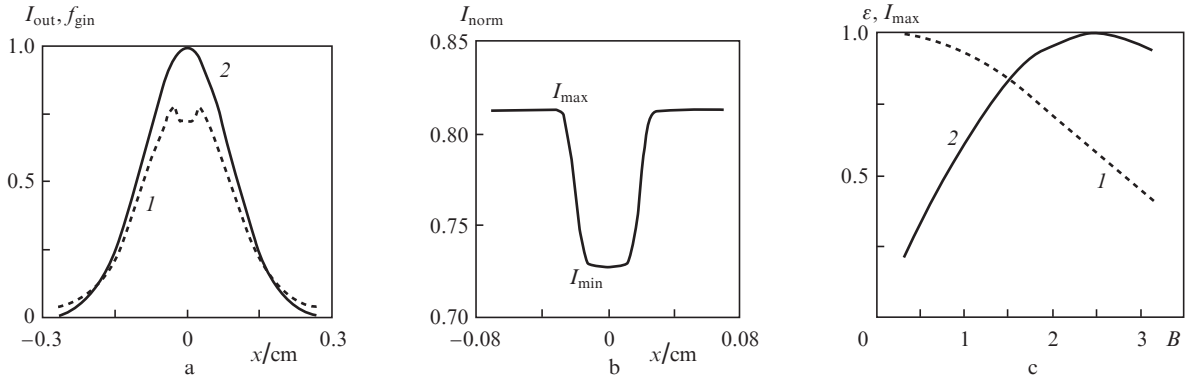

Figure 5. Characteristics of the process of the phase slit visualisation using a Zernike cell with cubic nonlinearity. Intensity distributions in the image plane, obtained upon visualisation of the phase slit I_{out} (slit phase jump $\varphi_0 = -0.1$ rad, width $d_{sl} = 0.04$ cm, parameter $B = \pi/2$) (*1*) and in the absence of the phase slit and the Zernike filter f_{gin} (*2*) (a). Normalised intensity distribution $I_{norm}(x)$, obtained upon the phase slit visualisation with the slit width $d_{sl} = 0.04$ cm, the phase jump $\varphi_0 = -0.1$ rad, and the parameter $B = \pi/2$ (b). Dependences of the maximal intensity value I_{max} (*1*) and the transfer constant ε (*2*) on the parameter B (c).

the thermal Zernike cell. The Rayleigh criterion is commonly accepted for this aim [2, 4, 5], following which two objects are considered as resolved if the following condition is satisfied

$$\theta_0 = \frac{d}{z} = 0.61\frac{\lambda}{r_{len}}. \quad (8)$$

Here d is the separation between the objects; z is the distance between the objects and the lens; θ_0 is the angular separation between the objects; r_{len} is the aperture radius of the lens. This criterion is valid under the incoherent illumination of objects. In the case of two holes in a non-transparent screen, illuminated with incoherent light, condition (8) means that in the image plane the ratio of the central intensity I_0 to the maximal intensity I_{max} in the characteristic double-peak light distribution amounts to 0.735. If the two holes are coherently illuminated with a plane wave normally incident on the screen, the resolution is worse, provided that all other conditions are similar. Let us accept the condition $I_0/I_{max} = 0.735$ as a criterion of resolution. Then for coherent illumination the resolution condition (8) will be replaced with the condition [2]

$$\theta_0 = \frac{d}{z} = 0.82\frac{\lambda}{r_{len}}. \quad (9)$$

For the analysis of resolution of a thermal Zernike cell we will rely on criterion (9). As an object we take two 'phase holes', illuminated with a Gaussian beam. Within the phase holes the phase of the illuminating beam experiences the jump $\varphi_0 = -0.1\pi$, while outside the holes the phase is zero. The object is assumed to be located at the distance $z = 400$ cm from the lens having the focal length $f = 100$ cm. The radii of the holes are $r_0 = 0.014$ cm, the separation between the holes is $d = 0.056$ cm, the radius of the illuminating Gaussian beam is $w_0 = 0.09$ cm, and the sampling increment is 35 μm. The thermal Zernike cell with the parameter $B_T = 0.15$ is placed in the focal plane of the lens. The image function of the phase object $\Phi(x, y)$, reconstructed following the procedure described in the beginning of Section 3, takes both positive and negative values. In order to plot the image Φ, let us complete it with a constant: $\Psi = \Phi - \min(\Phi)$, $\Psi \geqslant 0$. Figures 6a and b present the distributions $\Psi(x, y)$, obtained at $r_{len} = 0.184$ and 0.276 cm, respectively. At $r_{len} = 0.184$ cm the Rayleigh resolution criterion is rigorously fulfilled, while the value $r_{len} = 0.276$ corresponds to weakening of the criterion by 50%. In Figs 6c, d ($r_{len} = 0.184$ and 0.276 cm, respectively) the solid curves present reconstructed distributions of the phase $\Phi(x)$ in the cross-section plane $y = 0$. The dashed curves in these figures correspond to the distribution of the original phase object. Based on the analysis of Fig. 6 one can arrive at the following qualitative conclusion: the thermal Zernike cell allows phase object reconstruction with the resolution, close to the Rayleigh one.

The problem of resolving the considered phase object is more complicated than the traditional problem with a non-transparent screen with holes (amplitude object). The reason is the difference in image contrast. Phase objects produce less contrast images than the amplitude screen. The image contrast for a phase object depends on the phase jump φ_0. The greater is this jump, the easier is the solution (at least, visual) of the resolution problem. However, the value of φ_0 is limited by the linear part of the transfer characteristic (see Fig. 4). In the numerical experiment carried out by us $\varphi_0 = -0.1\pi$ and stays within the linear part of the transfer characteristic. In spite of the problems listed, one can state that the observed resolution of the transparent object visualisation system with thermal Zernike cell is close to the resolution, corresponding to the Rayleigh criterion (9).

4. Conclusions

The analysis of the calculated images shows that, generally, the images visualised using the photothermal Zernike cell reproduce the structure of small-scale phase objects quite well. The nonlocality of the response, typical of thermal nonlinearity, leads to low-frequency distortions (edge enhancement effects) that become reduced as the size of the phase object decreases. The transfer characteristic of the cell depends on the parameter B_T that determines the phase shift introduced by the cell. This parameter allows relatively easy control by changing the power of the laser beam, illuminating the object. Particularly, at $B_T = 0.1-0.25$ a quite satisfactory dynamical range of the transfer characteristic linear part ($|\Delta\varphi| \leqslant 1$) is achieved in the cell, the transfer constant (contrast) being $\varepsilon \sim 1$. In principle, the process of thermal self-action can disturb the visualisation process, but at ($|\Delta\varphi| \leqslant 1$) their manifestations are minor. The thermal cell demonstrates high resolution in imaging of small-scale details. Its resolution power is near to the Rayleigh one.

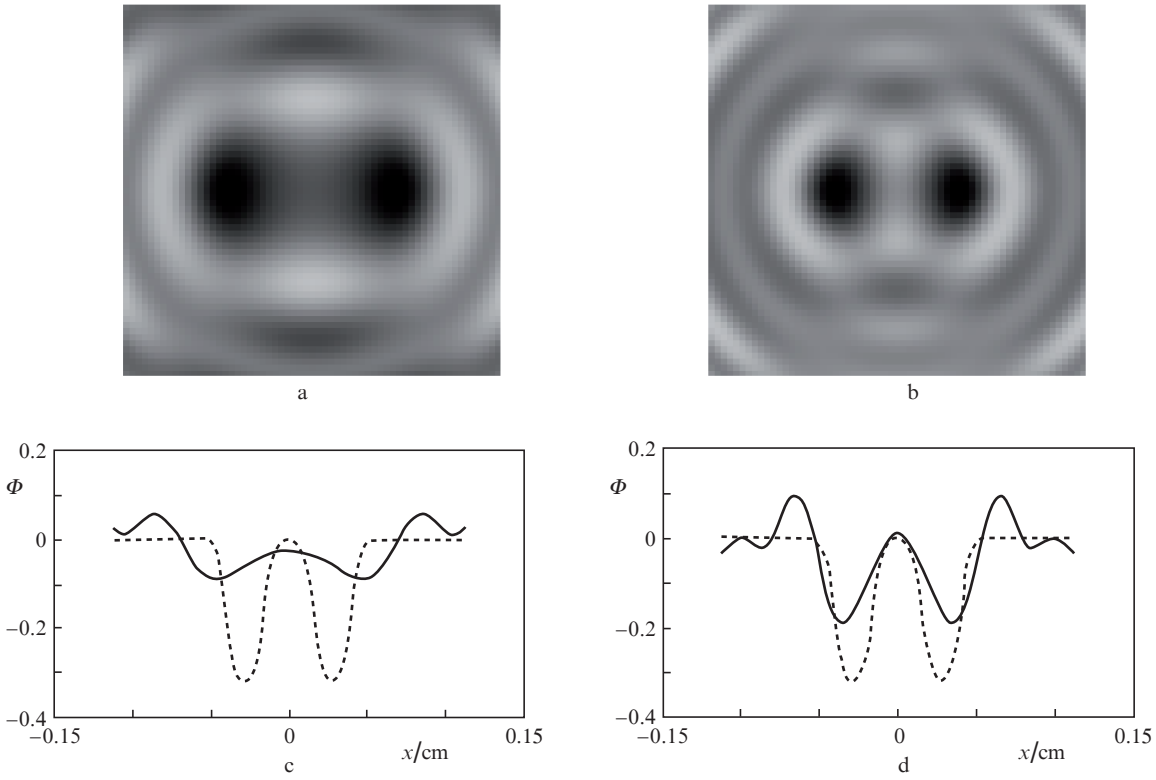

Figure 6. Resolution of a photothermal Zernike filter. Visualisation of two phase holes using a finite-aperture lens. Distributions of the 'displaced' image of the phase $\Psi(x, y)$, obtained at $r_{\text{len}} = 0.184$ (a) and 0.276 cm (b). Distributions of the reconstructed phase $\Phi(x, y = 0)$ (solid curve) and the initial phase (dashed curve), obtained at $r_{\text{lens}} = 0.184$ (c) and 0.276 cm (d).

References

1. Zernike F. *Physica*, **9** (7), 686 (1942).
2. Born M., Wolf E. *Fundamentals of Optics* (London: Pergamon, 1959; Moscow: Nauka, 1973).
3. Vorontsov M.A., Koryabin A.V., Shmalhausen V.I. *Upravlyaemye opticheskiye sistemy* (Controlled Optical Systems) (Moscow: Nauka, 1988).
4. Maréchal A., Françon M. *Diffraction Structures des Images* (Paris: Masson, 1960; Moscow: Mir, 1964).
5. Goodman J. *Introduction to Fourier Optics* (New York: McGraw Hill, 1996; Moscow: Mir, 1970).
6. Chernega N.V., Brekhovskikh G.L., Kudryavtseva A.D., et al. *Kvantovaya Elektron.*, **16**, 2530 (1989) [*Sov. J. Quantum Electron.*, **19**, 1626 (1989)].
7. Yelleswarapu Ch.S, Kotapalli S.-R., Aranda F.J., et al. *Appl. Phys. Lett.*, **89**, 211116-1 (2006).
8. Trevino-Palacios C.G., Castillo V.D.I., Sanchex-de-la-Liave D., et al. *Appl. Opt.*, **42** (25), 5091 (2003).
9. Bubis E.L. Preprint of the Institute of Applied Physics, RAS, No. 698 (N. Novgorod, 2006).
10. Bubis E.L., Matveev A.Z. *Pis'ma Zh. Tekh. Fiz.*, **33**, 8 (2007) [*Tech. Phys. Lett.*, **33**, 454 (2007)].
11. Bubis E.L. *Prib. Tekh. Eksp.*, (1), 119 (2009) [*Instruments and Experimental Techniques*, **52** (1), 108 (2009)].
12. Pushpa A. K., Vijayan C. *Appl. Opt.*, **48** (28), 5259 (2009).
13. Komorowska K., Miniewicz A., Parka J., et al. *J. Appl. Phys.*, **92** (10), 5635 (2002).
14. Bubis E.L. *Kvantovaya Elektron.*, **41** (6), 568 (2011) [*Quantum Electron.*, **41** (6), 568 (2011)].
15. Bubis E.L., Matveev A.Z. Preprint of the Institute of Applied Physics, RAS, No. 737 (N. Novgorod, 2007).
16. Bubis E.L. *Pis'ma Zh. Tekh. Fiz.*, **34** (12), 29 (2008) [*Tech. Phys. Lett.*, **34** (6), 510 (2008)].
17. Stein A. *IEEE J. Quantum Electron.*, **10** (4), 427 (1974).
18. Abramovitz M., Stigan I.M. *Handbook of Mathematical Function* (New York: Dover, 1965).
19. Bubis E.L., Potyomkin A.K., Shubin S.V. *Opt. Spektrosk.*, **90**, 336 (2001) [*Opt. Spectrosc.*, **90**, 288 (2001)].